ELSEVIER

Contents lists available at ScienceDirect

Inorganica Chimica Acta

journal homepage: www.elsevier.com/locate/ica



Research paper



An *in-situ* SAXS approach to probe stratification during drying of inorganic nanoparticle films

Weiping Liu, Jiachun Shen, Surita R. Bhatia

Department of Chemistry, Stony Brook University, Stony Brook, NY 11794-3400, USA

ARTICLE INFO

Keywords: Nanoparticle Stratification Evaporative assembly Films

ABSTRACT

Understanding particle motion during drying of colloidal and nanoparticle mixtures can be of great significance to processes such as stratification during film formation. Much of the current research in this field focuses on theory and simulation; however, additional experimental approaches are needed to support these studies. Here, we report a novel way to study film structures by applying an *in-situ* small angle X-ray scattering (SAXS) approach. We present studies of binary films containing two different sizes of silica particles. Our analysis allows us to probe the difference in particle packing in different layers and at different drying times. Furthermore, we can compare film samples consisting of particles with different initial concentrations and size ratios. Although the sample series presented here is limited, the data demonstrates proof-of-concept of the experimental technique. The method will be beneficial for future studies of structure formation in relatively thick films containing inorganic nanoparticles.

1. Introduction

Functional coatings are critical for many industrial applications and thus are in increasing demand for a variety of purposes, such as antibacterial coatings, anti-mold coatings, and so on [1-3]. Under many of these circumstances, multicomponent film fabrication is utilized to achieve a layered coating with desired properties at the interfaces. There are currently some attempts to make multi-layered films via a single-step deposition of mixtures of materials followed by evaporation of solvents, while traditional processes rely on only one layer of materials being applied at a time, which is not as time- or cost-effective as a single-step process.

The understanding of how different particles migrate during evaporation is of great importance. Theory by Routh and Russel [4–6] purposed that colloidal particle motion during film formation is determined by the Peclet number (Pe) where the competition is quantified between evaporation and Brownian motion:

$$Pe = \frac{6\pi\eta RHE}{kT} \tag{1}$$

where η is the solvent viscosity, R is the particle radius, H is the initial film thickness, E is the rate of evaporation, k is Boltzmann's constant, and T is the temperature. They predicted that, as the solvent front moves

down during evaporation, particles are able to diffuse away and distribute uniformly in the mixture when diffusion dominates (Pe \ll 1) or remain trapped at the air-film interface when evaporation dominates (Pe \gg 1). Furthermore, Trueman et al. suggested that having particles with two different sizes so their Pe straddle unity can encourage stratification, where large particles enrich the top of final dried film and small particles enrich the bottom [7]. This is sometimes referred to as a "large-on-top" structure (Fig. 1).

Many recent studies have a different observation of inverted stratification, with small particles enriched at the top surfaces of dried films. This has also been referred to as "small-on-top" stratification (Fig. 1). These studies focused on film formation under fast evaporation condition (Pe $\gg 1$ for both particles). Fortini et al. [8] believed the inverted stratification can be a result of differences in an osmotic pressure gradient between particles, while Panagiotopoulos et al. [9] attributed it to chemical potential gradient differences. Other studies of Zhou et al. [10] further discovered that various stratification states with large particles on top, with small particles on top, and no stratification (uniform distribution) are all possible scenarios depending on drying conditions, particle size ratios and particle volume percentages.

Much of the recent research of this phenomenon has been supported by computational simulations, which have some limitations such as difficulties in correctly estimating interactions between particles and

E-mail address: surita.bhatia@stonybrook.edu (S.R. Bhatia).

^{*} Corresponding author.

solvent. These models generally neglected hydrodynamic effects and treated the continuous phase as a liquid with a certain viscosity, while Sear and Warren's diffusiophoresis model [11,12] explicitly considered hydrodynamic effects. Relatively few experiments have been performed to investigate dried film structures. Atomic force microscopy (AFM) has been one of the most widely used approaches to investigate the surface compositions. Both large and small particles enriched at the top surfaces were observed via AFM under different drying conditions [13–15]. However, AFM can only characterize a limited area and only be applied at or near the film upper surface. Moreover, the composition of the upper surface may be affected by interfacial interactions. Depthresolved composition of dried films becomes important to the understanding of the stratification mechanism, yet these experiments are difficult to perform. Cryo-SEM and conventional SEM have been used to characterize the film structure during drying [14], though this possesses difficulties in quantification and preventing artifacts. Confocal microscopy, which was used by Fortini et al. [8], can be applied, although this technique also poses challenges in quantifying the results. Baesch et al. recently utilized three-dimensional Raman spectroscopy to study the composition and morphology of dry films [16].

Recently, our group performed microbeam small-angle X-ray scattering (SAXS) experiments on dried colloidal films and quantified the final compositions [17,18]. In these experiments, a micro-focused beam was applied to a very small thickness (\sim 20 μ m) of colloidal films and samples were moved along the vertical direction to analyze the depthresolved structures. Intensity differences were obtained and further quantified. Interestingly, in addition to large-on-top and small-on-top stratification, our group also discovered "sandwich" structures (Fig. 1), where one type of particle was enriched at both the top and bottom surfaces, and the other particle was enriched at the center. These

"sandwich" structures had not be discussed in detail previously, although there is some evidence that similar types of structures were observed in earlier experiments and simulations [19,20].

In order to learn more about the process of stratification, we developed an approach for in-situ measurements of film composition during the drying process. We designed a SAXS experimental system where wet samples were consistently heated until they dried, and we performed conventional SAXS at different positions within the samples by moving them along the vertical direction. To our knowledge, this type of approach has not been used previously to study stratification of multicomponent systems in situ during the drying process. These experiments are best performed on films that contain inorganic nanoparticles, which ensure sufficient intensity of the scattered X-ray beam. We elected not to focus the beam down for this series of experiments, as the wet films have a relatively large initial thickness (about 16 mm). The downside of this approach is that the final dried film becomes too thin to be studied with the relatively wide X-ray beam. If desired, the approach could be modified and performed with a narrow microbeam instead, and fewer data points taken in the early stages of drying. In either case, the X-ray scattering spectra from different depths of film during drying can be obtained and compared.

2. Experiment

Silica dispersions, purchased from Nanocomposix, Sigma-Aldrich and Grace, were used as provided or after necessary dilution with deionized water. Information on particle sizes is given in Table 1. The Peclet number is calculated based on water viscosity at 60 $^{\circ}\text{C}$ and a solvent evaporation rate measured during the SAXS experiments, as described below.

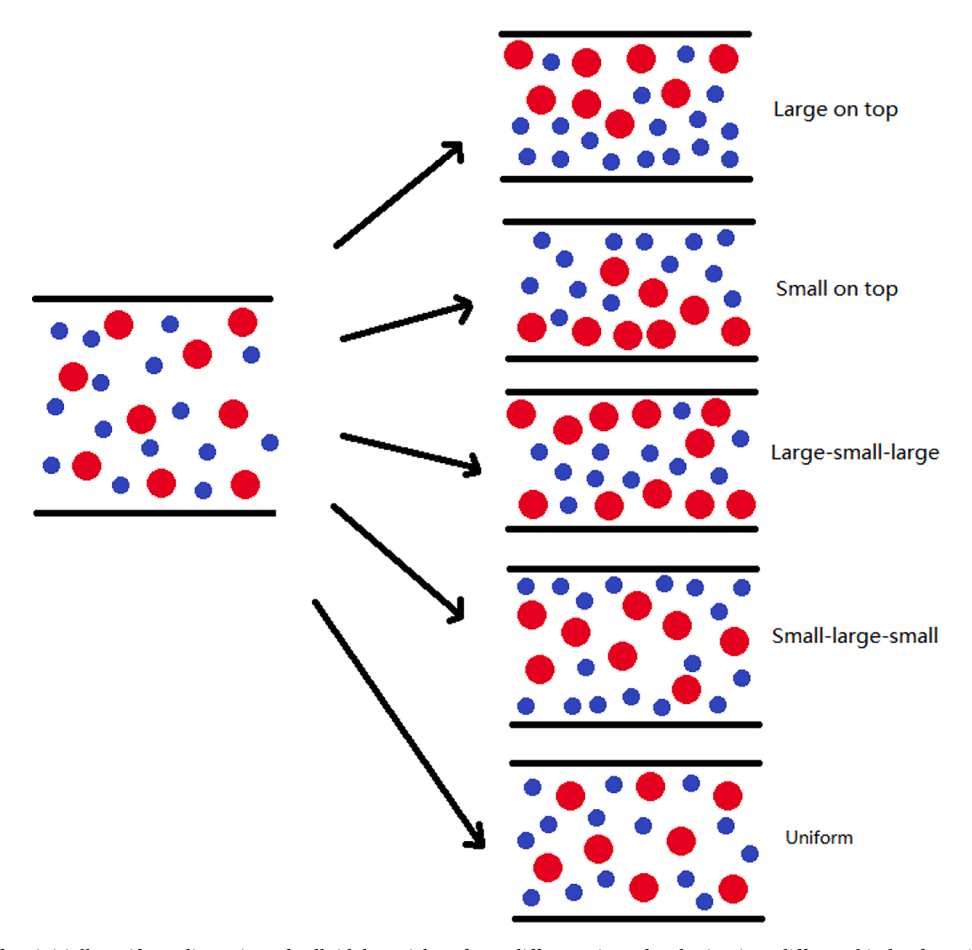


Fig. 1. An illustration of an initially uniform dispersion of colloidal particles of two different sizes, developing into different kinds of stratified/uniform dried films during solvent evaporation.

Table 1
Characteristics of silica particles and processing conditions used in this study.

Name	Radius (nm)	Peclet Number	LOT# and Supplier	Volume Concentration (as received)	Zeta Potential (mV)
Silica- 112	111.7 ± 0.8	527	JDR0029, Fisher Scientific	0.38%	-12.8 ± 2.9
Silica- 17	$17.8 \pm \\1.8$	94	MKBZ5447V, Sigma-Aldrich	15.09%	-57.4 ± 2.9
Silica- 6	$\begin{array}{c} \textbf{6.2} \pm \\ \textbf{0.2} \end{array}$	33	2017850358, Grace	15.47%	$-57.2 \pm \\4.5$

We paired different samples to achieve different particle size ratios as well as different initial volume percentage (from 0.19% to 1.9% diluted with de-ionized water). Single-component samples, which have one kind of particles with equivalent concentration as in binary mixtures, were also measured for data reduction and analysis. Information on mixed binary samples is given in Table 2. The particle size and initial volume percentage is shown as particle-radii (nm)-volume percentage (%) under columns "Particle 1" and "Particle 2", e.g. silica with radii as 112 nm and initial volume percentage as 0.19% is shown as Silica-112–0.19.

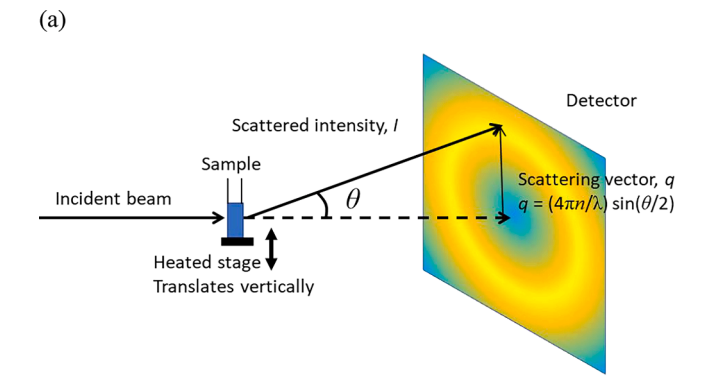
In-situ SAXS experiments were performed at the Complex Materials Scattering beamline (CMS, 11-BM) at the National Synchrotron Light Source II (NSLS-II), Brookhaven National Laboratory (BNL). X-rays with energies ranging from 10 to 17 keV were delivered by a 3-pole wiggler source. X-ray beams pass through a double multilayer monochromator, a toroidal focusing mirror, and a series of beam-defining and conditioning slits. Samples were placed in BrandTechTM BRANDTM plastic cuvettes with dimensions shown in Fig. 2. The beam passes through the narrow section of the cell, while the large opening at the top enables solvent evaporation over a reasonable time scale. These cuvettes were selected to obtain a small path length for the beam within the gel while still allowing for solvent evaporation. Cuvettes were supported by a sample holder with heating from the bottom. The sides of the cuvettes were wrapped in Kapton tapes to ensure good heat insulation and transparency in X-ray scattering. The top openings of cuvettes were exposed to the air to allow evaporation. Temperature was maintained at 60 °C, which allowed the samples to be completely dried in about 17–20 h. The sample holder was moved perpendicular to the X-ray beam direction, and SAXS data was collected throughout each sample at a vertical spacing of 0.5 mm, at different points in the drying process. This experimental set-up, where different positions in the film are achieved by moving the sample stage, ensures that the path length through the film is the same at all film depths measured. The detector distance was set to 5 m. The evaporation rate can be estimated by calculating the downward moving velocity of the solvent front, which was found to be 2.05×10^{-7} m/s, using the experimentally-measured time for complete evaporation of the solvent of 17.2 h at 60 °C for a representative sample. This was used to calculate the Pe values listed in Table 1.

3. Results and discussion

In-situ SAXS experiments yield scattering spectra at different depths within the drying films. In Fig. 3, we show scattering curves at a depth of approximately 0.5 mm beneath the top interface. We did not choose the topmost layer to analyze because this first data point often has some

Table 2 A list of mixture samples with the information of particle sizes and initial volume percentage ratio.

Name	Particle 1	Particle 2	Size Ratio	Volume Ratio
Mixture 1	Silica-112-0.19	Silica-6-1.9	18.0	1:10
Mixture 2	Silica-112-0.19	Silica-6-0.95	18.0	1:5
Mixture 3	Silica-112-0.19	Silica-17-1.9	6.3	1:10



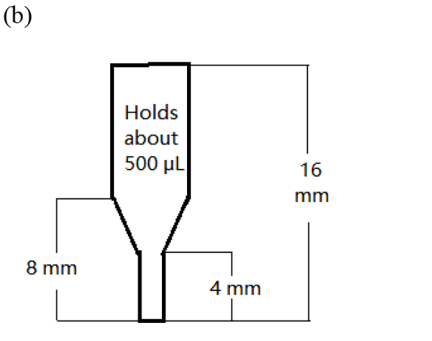


Fig. 2. (a) An illustration of SAXS experiment set up. (b) A sketch of the cross section of the sample cells used in these measurements, with dimensions.

edge effects from the beam not being fully in the film, and thus the intensity cannot be compared to data taken at other depths. SAXS scans are taken at different time points during the drying process, and we normalize these by the time it takes to fully dry the film; so for example, a film that is labelled 13% dry is at a time point that is 0.13 times the time it takes to fully evaporate the solvent. An estimate of the average uncertainty in the scattered intensity I can be estimated as $I_{err} = [err_{shot}^2]$ $+ err_{std}^2$, where err_{shot} is the Poisson-like "shot noise error" associated with photon counting statistics for a signal of a given intensity in the 1D average curve, and errstd is the standard deviation of the 2D data along an arc at a particular q. This does not account for the fact I has been averaged over multiple detector pixels and over the time of the measurement, and thus provides an upper-bound on the error in *I*. Using this approach, the relative error in *I* was found to be approximately 1.4% for Mixture 1 at the 76% dry state in the q range 2.99×10^{-3} to 1.80×10^{-1} \mathring{A}^{-1} .

Fig. 3 shows a series of SAXS data taken on Mixure 1 at time points ranging from 13% dry (red) to 92% dry (blue). As the solvent evaporates, the overall scattered intensity and the characteristic features from the particle form factors increase due to loss of solvent, and a peak corresponding to the structure factor appears, as expected. Much of the remaining discussion focuses on films that are 76% dry, at which point the majority of solvent has been removed. We are aware that there is still a significant amount of solvent remaining at this point in the drying process, but the resolution of this experiment does not allow us to probe film thickness smaller than X-ray beam size, i.e. fully or nearly dried films at the very end of the evaporation process.

In order to study the stratification process for drying silica dispersions, we plot the scattered intensity of Mixture 1 at different depths for films that are 76% dry in Fig. 4(a), where 10% is near the top (0%) and 90% is near the bottom interface (100%). However, no obvious difference is observed, other than upper layers having a slightly higher intensity than the lower layers in some regions of the curve. Similarly, if we compare these mixture data to the curves measured on a single-component film of Silica-112 (Fig. 4b), we also see barely any difference in the scattered intensity at different depths at 76% drying time. If

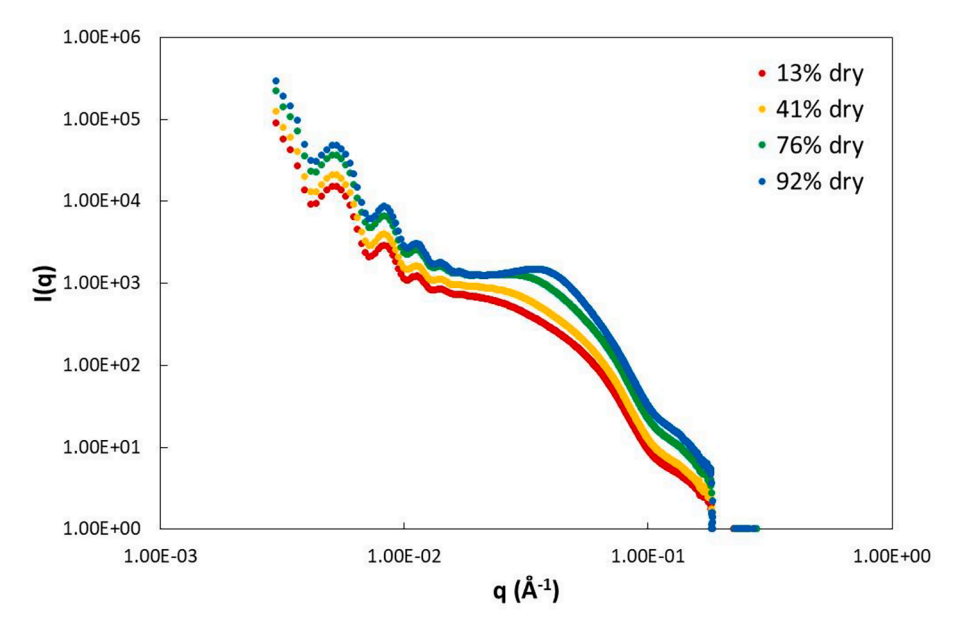
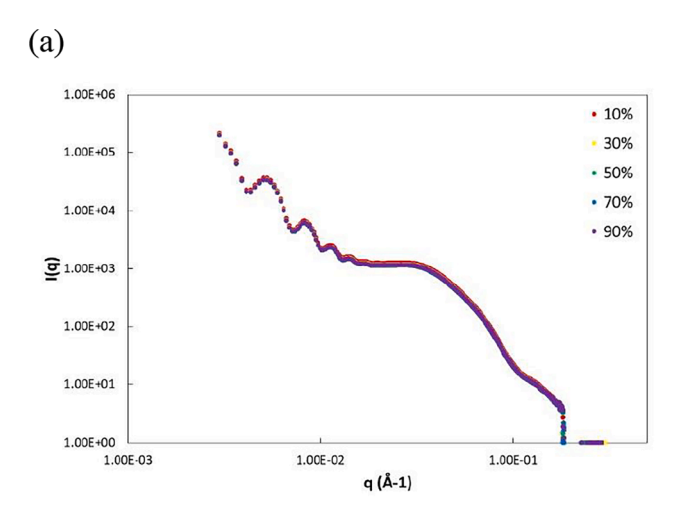


Fig. 3. Scattered intensity versus scattering vector q for the top 0.5 mm thickness of Mixture 1 at different representative drying times, from 13% to 92% dry.



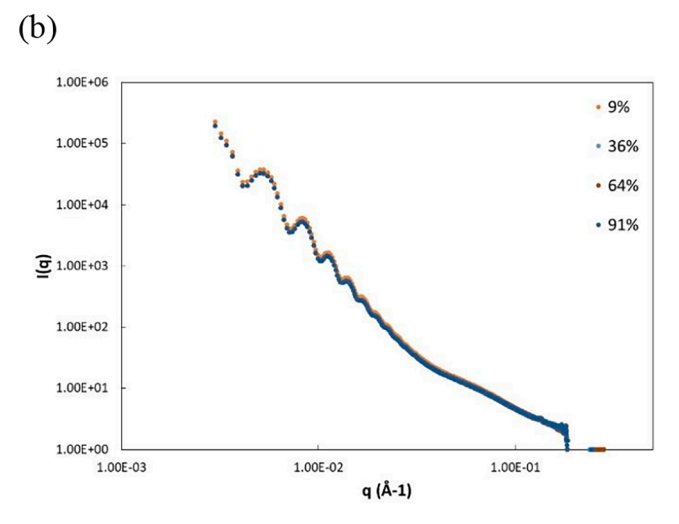


Fig. 4. Scattered intensity versus scattering vector q on a log–log scale for (a) Mixture 1 and (b) Silica-112-0.19 at different film depths, at 76% dry time. 0% and 100% depth layers are defined as top and bottom interface, respectively.

there is a weak variation in the structure with film depth, it is difficult to discern by looking at the total scattered intensity. This leads to the residual-type analysis described in the next section.

To highlight scattering from one component in the binary mixture, we assume that the intensity of the binary mixture can be expressed as a linear combination of two individual components, and perform further analysis of the data by subtracting data taken on films containing one type of particle from the data taken on the binary mixtures. This assumption should be valid for the disordered, partially dried suspensions in this study. As drying proceeds, the impact of packing of two different particle types can give rise to local configurations, and thus scattering features, that are not present in the pure systems. We have not considered the very late stages of drying in this work. Thus, for the systems studied here, we expect that a linear combination of the pure material scattering curves provides a reasonable approximation to the total scattering curve.

Fig. 5 shows the residual intensity of Silica-6 in Mixture 1, obtained by subtracting the measured intensity of Silica-112 from the Mixture 1 data at the equivalent drying times and film depths. Interestingly, we observe regular peaks in the low q range, suggesting a well-ordered structure, that are not seen in the total scattered intensity from the mixture (Fig. 4). These peaks shift to a higher intensity and lower q as we proceed into deeper layers of the film. These are at a lower intensity than the intensity from the mixture, which explains why these characteristics are not readily apparent in Fig. 4.

Comparing the residual scattering of Silica-6 with those of Mixture 1 and Silica-112, the low q features do not necessarily match the positions of features seen in the form factors for larger silica particles, while the high q features overlap nicely in terms of both positions and intensity scales. In the residual intensity curves of Silica-6, we can see that the heights and positions of these peaks at low q vary with film depth. Layers closer to the bottom of the film have higher intensity, and the peaks are shifted to lower q. We do not believe that these features are due to the formation of aggregates or clusters, but rather due to structural factors and interparticle correlations of Silica-6 that are present in the mixture but not in the single-component sample. These features become more prominent in the bottom layers of the mixed film, and this together with the shift in q suggests that there may be a change in concentration of Silica-6 as we move through the bottom layers of the film. Additionally, the high q features that correspond to form factor of Silica-6 particles are of slightly lower intensity for deeper layers but do not show an obvious

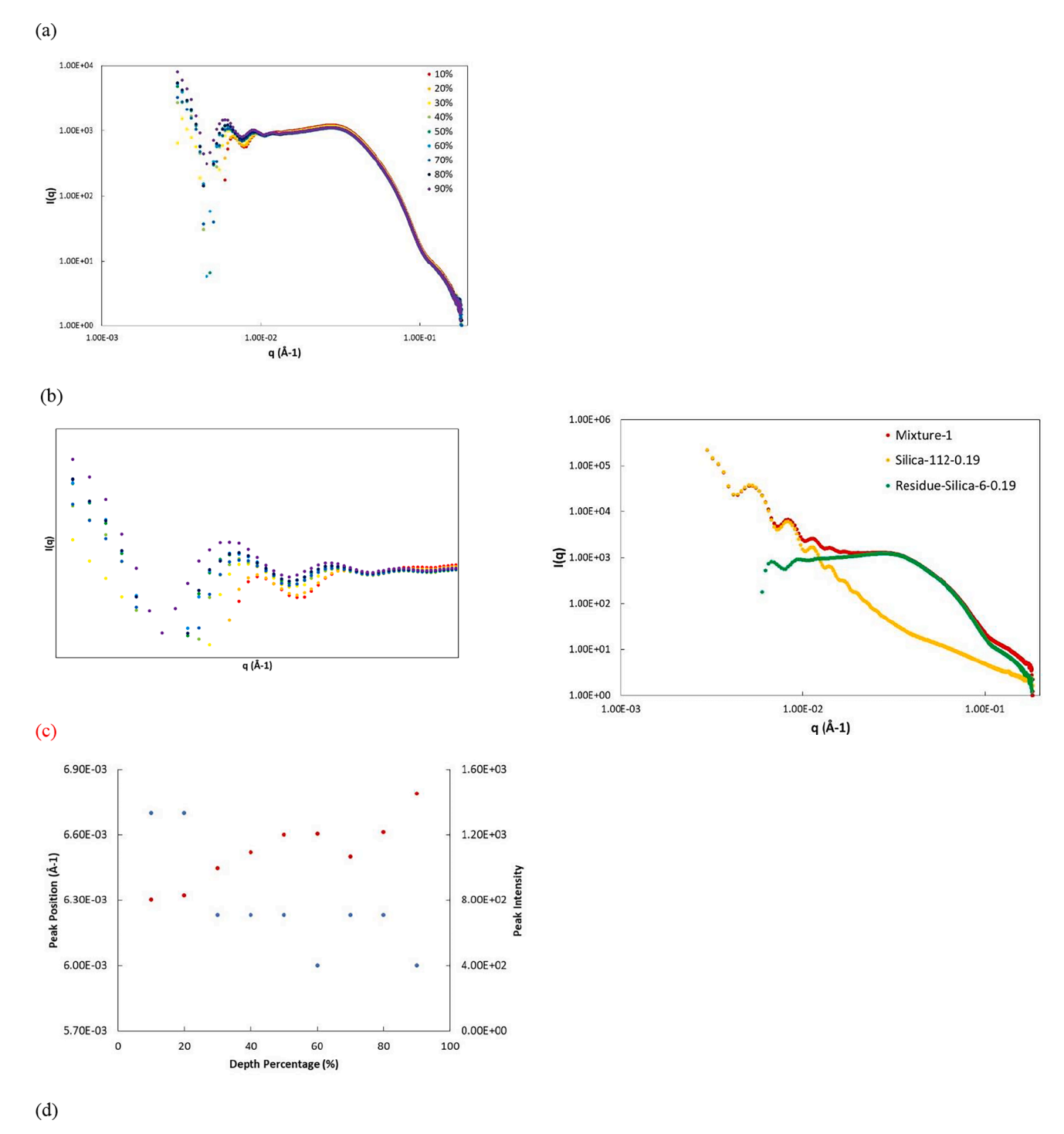


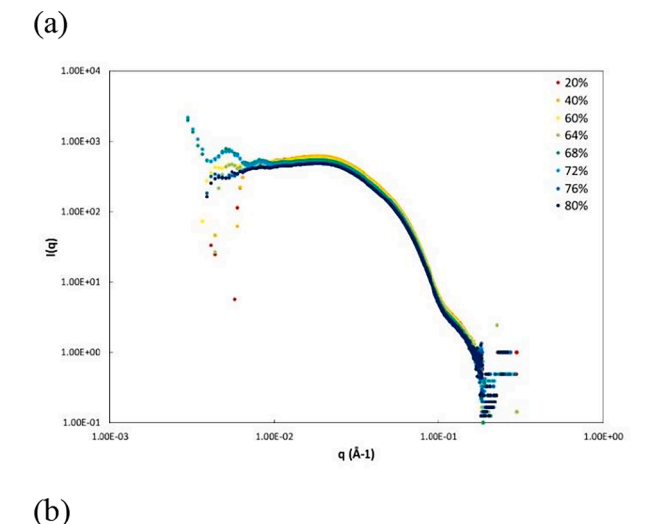
Fig. 5. (a) Residual scattered intensity versus scattering vector q on a log-log scale for Silica-6 in Mixture 1 at different film depths, at 76% dry time. The 0% and 100% depth layers are defined as top and bottom interface, respectively. (b) Enlarged view of low q peaks in the residual intensity, of Silica-6. Symbols are the same depths as indicated in (a). (c) Position (blue) and residual intensity (red) for the first defined peak in (b) at different depth. (d) Scattered intensity versus scattering vector q on a log-log scale for Mixture 1, Silica-112 and residual scattering from Silica-6 at a depth close to top interface, at 76% dry time. (For interpretation of the references to colour in this figure legend, the reader is referred to the web version of this article.)

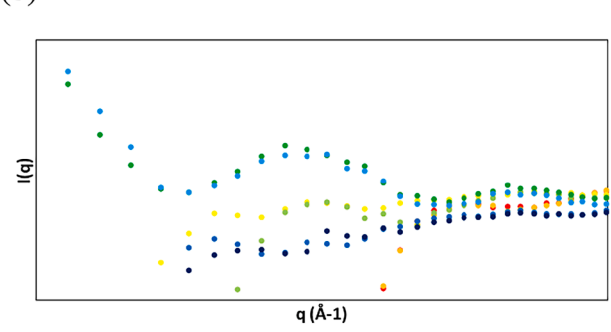
difference in positions.

In Fig. 6, we plot the residual intensity of Silica-6 for different depths at 13% dry time, obtained in the same way as above. The variations in peak positions are clearly weaker than in the 76% dry film. At this earlier stage of drying, we only observe some features near the bottom of the film, at depths between 68 and 72%. Based on this observation, for these particles and evaporation conditions, it appears that stratification may first become apparent in the bottom of the film. This is somewhat

surprising, as we would normally expect that stratification effects would first occur in the upper part of the film, near the drying front.

According to a previous computational study by Zhou et al., both the initial concentration of small particles and particle size ratio play an important role in stratification of drying binary mixtures [10]. They proposed a boundary condition for small particles to enrich the top surface, $\alpha^2(1+\text{Pe}_1)\varphi_{01}>1,$ where α is particle size ratio, Pe $_1$ is Peclet number for small particle and φ_{01} is the initial concentration for small





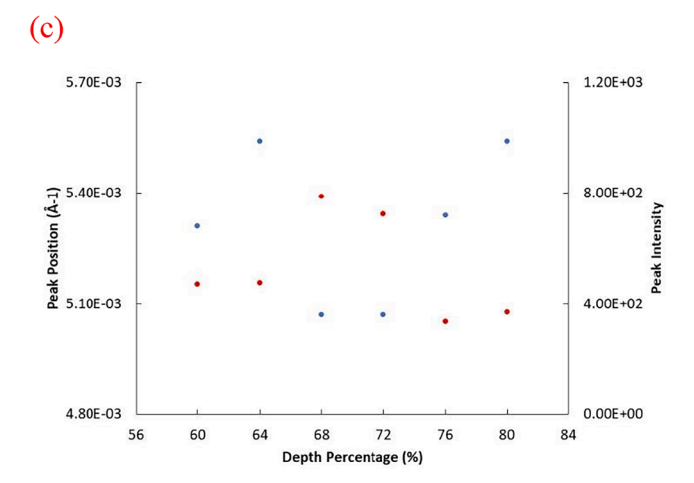
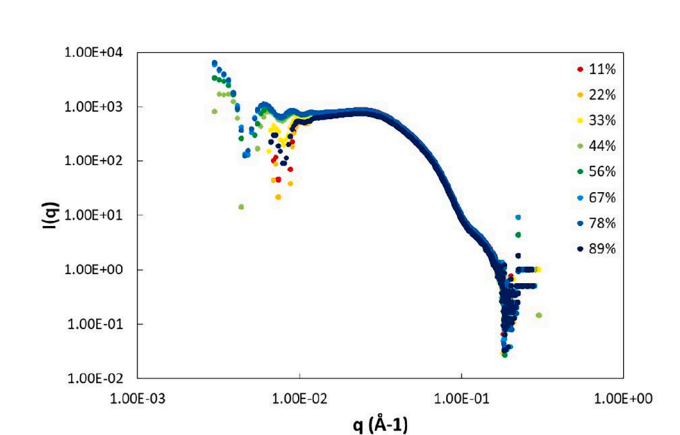


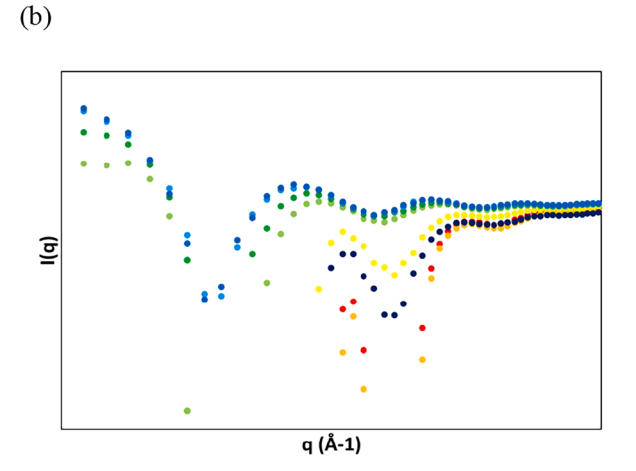
Fig. 6. (a) Residual scattered intensity versus scattering vector q on a log-log scale for Silica-6 in Mixture 1 at different film depths, at 13% dry time. The 0% and 100% depth layers are defined as top and bottom interface, respectively. (b) Enlarged view of low q peaks in the residual intensity, of Silica-6. Symbols are the same depths as indicated in (a). (c) Position (blue) and residual intensity (red) for the first defined peak in (b) at different depth. (For interpretation of the references to colour in this figure legend, the reader is referred to the web version of this article.)

particles. In our study, all systems are expected to have small on top stratification based on this model, while Mixture 1 should have the most stratified dried film because of the largest size ratio and small particle concentration used.

In order to probe the effect of small particle concentration, we compare the residual scattering from Silica-6 for Mixture 2 (Fig. 7), which has an initial volume percentage of Silica-6 of 0.95%, with Mixture 1, which has an initial volume percentage of Silica-6 of 1.9%, at



(a)



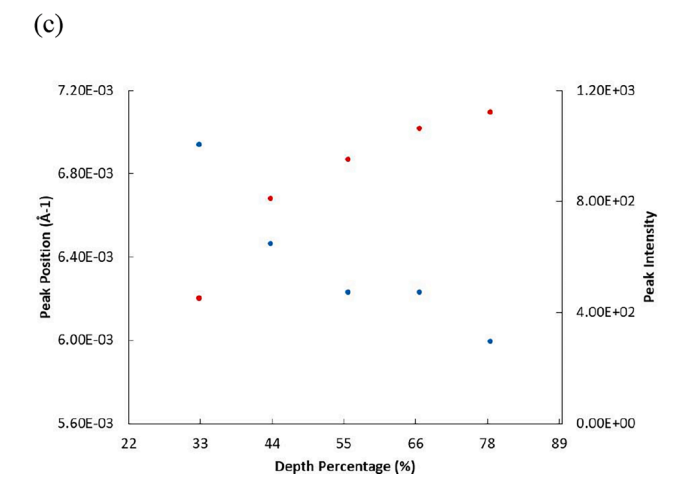


Fig. 7. (a) Residual scattered intensity versus scattering vector q on a log-log scale for Silica-6 in Mixture 2 at different film depths, at 76% dry time. The 0% and 100% depth layers are defined as top and bottom interface, respectively. (b) Enlarged view of low q peaks in the residual intensity, of Silica-6. Symbols are the same depths as indicated in (a). (c) Position (blue) and residual intensity (red) for the first defined peak in (b) at different depth. (For interpretation of the references to colour in this figure legend, the reader is referred to the web version of this article.)

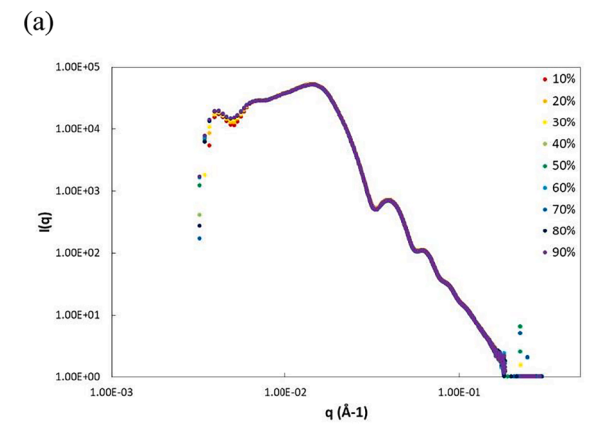
76% dry time. Similar to Mixture 1, the residual scattering from Silica-6 shows peaks in the low q range, and these peaks have the highest intensity for layers that are at 44-78% depth. The residual scattering intensity from Silica-6 increase as we proceed from top layer to bottom, but then drop at 89% depth, while the peak position shift to a lower q. This lower intensity at top suggests that the top layer to the film is less ordered. A right-shifted peak position at top indicates there is a larger spacing among particle arrangement. To compare these characteristics in Mixture 1 and Mixture 2, the variation in peak positions is similar. Nevertheless, the absolute intensity of residue peaks at low q are slightly higher for Mixture 1 showing a higher degree of ordering. A less defined development in intensity and peak position from top to bottom layer in Mixture 2 might be due to the competition of different effects on stratification and so that both interfaces end up becoming less ordered, which is believed to have the potential to cause "sandwich" structures where one type of particles enriches top and bottom layers and another enriches the center of a film. Although the intensity ratio between highest and lowest peaks is relatively large for Mixture 2, the highest peak appears near the center of the film and the intensity show a nonlinear trend from top to bottom layer, which is quite different from

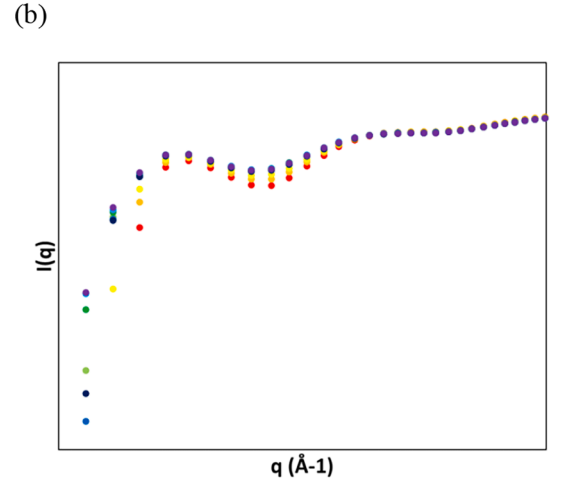
We also applied the technique to explore the effect of particle size ratio through Mixture 3, where the smaller Silica-17 particles are 17 nm in radius, and thus the size ratio is 6.3. Using the same analysis method, in Fig. 8 we show the residual scattering from the smaller particles, in this case Silica-17, from Mixture 3 at different depths for a sample at 76% dry time. Peaks are again observed in the low q regime, and they are of an order of magnitude higher in intensity than in Mixture 1 and Mixture 2, implying a stronger ordering effect in this film. However, the intensity differences at different depths are small, i.e. the ratio between the highest and the lowest peak is 1.13 for Mixture 3 but is 1.80 for Mixture 1. In addition, there is no clear variation in the form factor of Silica-17 particles. This implies that a smaller size ratio of particles in the binary mixture results in a relatively uniform arrangements throughout the film, e.g. no or minimal stratification, which is not surprising based on previous studies [9,10,13,14].

Although we do not observe strong stratification in the overall scattering intensity at different depths as predicted by the boundary condition predicted by Zhou et al., this study still see some differences in particle ordering for these films. However, it is possible for particles to rearrange themselves at a late stage of drying [21], and the technique we used here cannot probe film structures at that point. The development of understanding how to promote or diminish stratification, such as by controlling volume concentration ratio and particle size ratio, can guide the fabrication and application of multifunctional coatings; for example, fabrication of anti-bacterial coatings through the incorporation of silver particles at the top surface, or optical coatings through production of samples with a specified gradient in silica or another componenty throughout.

4. Conclusions

In-situ SAXS was applied to provide a novel method to study the stratification process in drying colloidal films consisting of different size particles. Although we examined binary mixtures of the same material with different particle sizes, the technique can be applied to mixed films of two different types of inorganic or ceramic materials, or to composite films containing both inorganic and organic particles. The scattering spectra of a fixed layer in the film at different drying times shows there is some difference in the particle ordering as drying proceeds. Because features of each particle can be difficult to discern when looking at the total scattered intensity, we examined the residual scattering from a single component within the mixture, obtained by subtracting the intensity from a drying film containing only the other component. Performing this type of analysis to highlight the scattering from small particles provided some insights into the effects of initial small particle





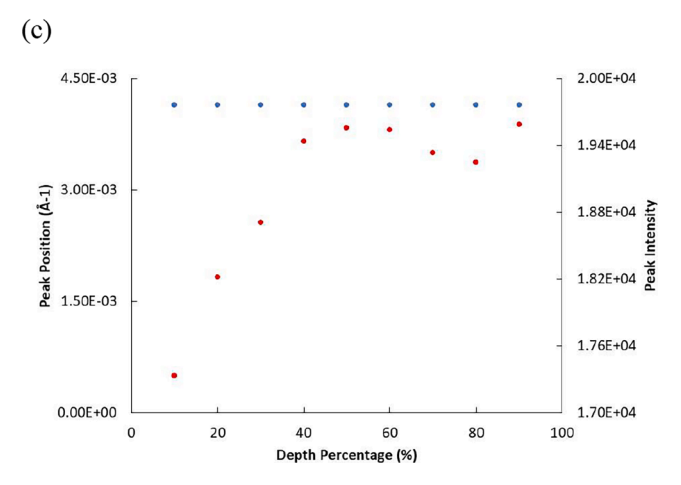


Fig. 8. (a) Residual scattered intensity versus scattering vector q on a log-log scale for Silica-17 in Mixture 3 at different film depths, at 76% dry time. The 0% and 100% depth layers are defined as top and bottom interface, respectively. (b) Enlarged view of low q peaks in the residual intensity, of Silica-17. Symbols are the same depths as indicated in (a). (c) Position (blue) and residual intensity (red) for the first defined peak in (b) at different depth. (For interpretation of the references to colour in this figure legend, the reader is referred to the web version of this article.)

concentration and particle size ratio. However, the overall variation of the particle distribution across the film depths appear to be less significant than expected, likely due to a large initial film height, long drying process, and high Peclet numbers.

This proof-of-concept study demonstrates the utility of in-situ SAXS experiments in studying stratification in thick films containing inorganic

nanoparticles. With the limited systems studied here, it is difficult to draw conclusive insight into the physics of the stratification process. However, future studies over a wider range of particle sizes and size ratios, as well as varying the sample cell and environment to enable a range of evaporation rates, is envisioned for future studies. In addition, the results can be integrated with complementary simulations of particle motion during drying to help verify predictions and provide directions for improving theoretical descriptions of evaporative assembly.

CRediT authorship contribution statement

Weiping Liu: Investigation, Formal analysis, Writing - original draft. Jiachun Shen: Investigation. Surita R. Bhatia: Conceptualization, Funding acquisition, Project administration, Supervision, Writing - review & editing.

Declaration of Competing Interest

The authors declare that they have no known competing financial interests or personal relationships that could have appeared to influence the work reported in this paper.

Acknowledgments

We thank the editors for organizing this special issue in honor and memory of Prof. Tara P. Dasgupta and for inviting our group to contribute. Financial support for this work was provided by National Science Foundation awards CBET-1903189 and DGE-1922639. This research used beamline 11-BM of the National Synchrotron Light Source II, a U.S. Department of Energy (DOE) Office of Science User Facility operated for the DOE Office of Science by Brookhaven National Laboratory under Contract No. DE-SC0012704. The sponsors had no role in the study design; in the collection, analysis and interpretation of data; in the writing of the report; and in the decision to submit the article for publication.

References

- D.M. Eby, H.R. Luckarift, G.R. Johnson, Hybrid antimicrobial enzyme and silver nanoparticle coatings for medical instruments, ACS Appl. Mater. Interfaces 1 (7) (2009) 1553–1560, https://doi.org/10.1021/am9002155.
- [2] P.A. Fulmer, J.H. Wynne, Development of broad-spectrum antimicrobial latex paint surfaces employing active amphiphilic compounds, ACS Appl. Mater. Interfaces 3 (8) (2011) 2878–2884, https://doi.org/10.1021/am2005465.
- [3] C. Zhang, X. Zhao, J. Lei, Y. Ma, F. Du, The wetting behavior of aqueous surfactant solutions on wheat (Triticum aestivum) leaf surfaces, Soft Matter 13 (2) (2017) 503–513, https://doi.org/10.1039/C6SM02387H.

- [4] A.F. Routh, W.B. Russel, Horizontal drying fronts during solvent evaporation from latex films, AIChE J. 44 (9) (1998) 2088–2098, https://doi.org/10.1002/ aic.690440916.
- [5] A.F. Routh, W.B. Russel, A process model for latex film formation: limiting regimes for individual driving forces, Langmuir 15 (22) (1999) 7762–7773.
- [6] A.F. Routh, W.B. Russel, Deformation mechanisms during latex film formation: experimental evidence, Ind. Eng. Chem. Res. 40 (20) (2001) 4302–4308.
- [7] R.E. Trueman, E. Lago Domingues, S.N. Emmett, M.W. Murray, A.F. Routh, Auto-stratification in drying colloidal dispersions: a diffusive model, J. Colloid Interface Sci. 377 (1) (2012) 207–212, https://doi.org/10.1016/j.jcis.2012.03.045.
- [8] A. Fortini, I. Martín-Fabiani, J.L. De La Haye, P.-Y. Dugas, M. Lansalot, F. D'Agosto, E. Bourgeat-Lami, J.L. Keddie, R.P. Sear, Dynamic stratification in drying films of colloidal mixtures, Phys. Rev. Lett. 116 (11) (2016), https://doi.org/10.1103/ PhysRevLett.116.118301.
- [9] M.P. Howard, A. Nikoubashman, A.Z. Panagiotopoulos, Stratification dynamics in drying colloidal mixtures, Langmuir 33 (15) (2017) 3685–3693, https://doi.org/ 10.1021/acs.langmuir.7b00543.s001.
- [10] J. Zhou, Y. Jiang, M. Doi, Cross interaction drives stratification in drying film of binary colloidal mixtures, Phys. Rev. Lett. 118 (10) (2017), https://doi.org/ 10.1103/PhysRevLett.118.108002.
- [11] R.P. Sear, Stratification of mixtures in evaporating liquid films occurs only for a range of volume fractions of the smaller component, J. Chem. Phys. 148 (13) (2018) 134909, https://doi.org/10.1063/1.5022243.
- [12] R.P. Sear, P.B. Warren, Diffusiophoresis in nonadsorbing polymer solutions: the Asakura-Oosawa model and stratification in drying films, Phys. Rev. E 96 (6) (2017), https://doi.org/10.1103/PhysRevE.96.062602.
- [13] X. Liu, W. Liu, A.J. Carr, D.S. Vazquez, D. Nykypanchuk, P.W. Majewski, A. F. Routh, S.R. Bhatia, Stratification during evaporative assembly of multicomponent nanoparticle films, J. Colloid Interface Sci. 515 (2018) 70–77.
- [14] D.K. Makepeace, A. Fortini, A. Markov, P. Locatelli, C. Lindsay, S. Moorhouse, R. Lind, R.P. Sear, J.L. Keddie, Stratification in binary colloidal polymer films: experiment and simulations, Soft Matter 13 (39) (2017) 6969–6980, https://doi. org/10.1039/C7SM01267E.
- [15] R.E. Trueman, E. Lago Domingues, S.N. Emmett, M.W. Murray, J.L. Keddie, A. F. Routh, Autostratification in drying colloidal dispersions: experimental investigations, Langmuir 28 (7) (2012) 3420–3428, https://doi.org/10.1021/la203075h
- [16] V.-A. Gracia-Medrano-Bravo, J. Gröne, S. Baesch, P. Scharfer, W. Schabel, Influence of particle shape on the drying regime maps for platelike particle–polymer composites, Langmuir 36 (22) (2020) 6245–6253, https://doi. org/10.1021/acs.langmuir.0c00942.
- [17] A.J. Carr, W. Liu, K.G. Yager, A.F. Routh, S.R. Bhatia, Evidence of stratification in binary colloidal films from microbeam X-ray scattering: toward optimizing the evaporative assembly processes for coatings, ACS Appl. Nano Mater. 1 (8) (2018) 4211–4217, https://doi.org/10.1021/acsanm.8b00968.s001.
- [18] W. Liu, A.J. Carr, K.G. Yager, A.F. Routh, S.R. Bhatia, Sandwich layering in binary nanoparticle films and effect of size ratio on stratification behavior, J. Colloid Interface Sci. 538 (2019) 209–217.
- [19] C.M. Cardinal, Y.D. Jung, K.H. Ahn, L.F. Francis, Drying regime maps for particulate coatings, AIChE J. 56 (11) (2010) 2769–2780, https://doi.org/ 10.1002/aic.12190.
- [20] Y. Tang, G.S. Grest, S. Cheng, Control of stratification in drying particle suspensions via temperature gradients, Langmuir 35 (12) (2019) 4296–4304, https://doi.org/10.1021/acs.langmuir.8b03659.s001.
- [21] T. Tashima, M. Yamamura, Two-step migration of particles in evaporating bimodal suspension films at high Peclet numbers, J Coat Technol Res 14 (5) (2017) 965–970, https://doi.org/10.1007/s11998-017-9946-1.